Cement 25 (2026) 100187

Contents lists available at ScienceDirect

Cement

journal homepage: www.sciencedirect.com/journal/cement

Optimising cement systems containing amorphous precipitated silica derived from olivine, limestone and gypsum

Pei B. Ong, Chenyang Li, Christopher Cheeseman, Hong S. Wong *

Centre for Infrastructure Materials, Department of Civil and Environmental Engineering, Imperial College London, London SW7 2AZ, United Kingdom

ARTICLE INFO

Keywords:
Olivine
Amorphous silica
Limestone
Gypsum
Low-carbon cements

ABSTRACT

Amorphous precipitated silica (APS) derived from olivine has potential to be used as a pozzolanic supplementary cementitious material, but high specific surface area reduces mix workability, accelerates sulphate depletion and decreases early age strength. This study investigates the feasibility of blending Portland cement with APS, limestone and gypsum to address these issues. Quaternary binders containing 5 – 20 wt.% limestone and 2 wt.% gypsum were prepared at CEM I: APS mass ratio of 8:2. Results show that limestone improves workability and early hydration reactions, while gypsum stabilises sulphate availability and promotes strength development. Mortars with a binder system containing 10 wt.% limestone with 2 wt.% gypsum show comparable workability and strength to control mortars. The research demonstrates that olivine-derived APS can be combined with limestone and gypsum to form a viable low-carbon cement with reduced clinker content.

1. Introduction

The demand for alternative supplementary cementitious materials (SCMs) is driven by the need to reduce the embodied carbon in concrete. Olivine ($(Mg,Fe)_2SiO_4$) is a mineral that can be processed to form amorphous precipitated silica (APS) and magnesium carbonate as a carbon negative by-product [1–5]. Previous research has shown that APS is a highly reactive SCM. APS derived from olivine produces cement-based materials with mechanical properties comparable to Portland cement (CEM I) samples [5–7]. However, the replacement of CEM I by APS is constrained by the high specific surface area (SSA) of APS which significantly reduces the workability of APS containing mixes [2,4–6,8–10].

The addition of superplasticisers allows APS replacement level of up to 30 wt.% to be used [5–7]. However, large superplasticiser dosages are required to cast mortars containing APS with high SSA ($> 200\ m^2/g$). Thermal treatment has been used to reduce the SSA of APS and improve the workability of APS-containing mortars [7]. Although this decreased SSA, the influence on workability and water demand were marginal. Alternative strategies are therefore required to address the high SSA of olivine derived APS.

Limestone enhances the hydration of cement through filler and nucleation effects, and this accelerates the formation of hydration products [11–15]. Limestone can chemically interact with aluminate phases and portlandite to form mono or hemicarbonate phases, an effect referred to as the chemical contribution of limestone [13,16–18]. Although research has not explicitly demonstrated consistent improvements in workability, the relatively low SSA of limestone compared to other supplementary cementitious materials promotes water redistribution within the fresh mix, improving flow properties. These studies have primarily focused on conventional cement and limestone calcined clay cement (LC^3) systems. The combined influence of limestone and olivine derived APS in cementitious systems has not previously been reported.

Gypsum is used to control the hydration of C_3A and prevent flash set [19–22]. The additional surface area introduced by SCMs enhances the hydration of C_3S, leading to increased formation of C-S-H gel [13]. This accelerates gypsum depletion through adsorption of sulphate ions onto C-S-H. To mitigate this, sulphate correction has been used in cement blends containing high-SSA SCMs such as in LC^3 systems. Early strength increment has been reported when gypsum is added at moderate amounts [23]. Our previous study suggests that the formation of additional ettringite may offset the low early age strength of cements containing 20 wt.% APS [24]. However, the effect of increased gypsum content in Portland cement systems blended with olivine-derived APS has not previously been investigated.

The aim of this study is to develop an optimised novel quaternary binder system composed of CEM-I PC, olivine-derived APS, limestone,

* Corresponding author.
E-mail address: hong.wong@imperial.ac.uk (H.S. Wong).

https://doi.org/10.1016/j.cement.2026.100187

Available online 16 June 2026
2666-5492/© 2026 The Authors. Published by Elsevier B.V. This is an open access article under the CC BY license (http://creativecommons.org/licenses/by/4.0/).

and gypsum. The hypothesis proposes that the fresh and hardened state properties of cementitious materials containing APS can be enhanced by blending small proportions of limestone and gypsum. The main contribution to knowledge from the systematic experimental work done is an enhanced understanding of underlying mechanisms governing the performance of such quaternary binder system. It is envisaged that a successful outcome of the research will improve the prospects of olivine-derived APS as a viable SCM to deliver low-carbon cementitious materials with satisfactory engineering performance.

2. Materials and methods

2.1. Materials

Olivine (supplied by Sibelco), Portland cement (CEM-I 52.5 N, Breedon Group plc., UK), limestone powder (LS, Heidelberg Cement) and gypsum ($CaSO_4{\cdot}2H_2O$, purity $\geq$ 99.9%, Sigma-Aldrich) were used in all experiments. A polycarboxylic ether superplasticiser (SP, ViscoFlow 3000, SIKA) was used to improve dispersion and workability. Siliceous sharp sand (Builders Depot) with a water absorption of ~0.77 wt.% was used in mortar samples.

Amorphous precipitated silica (APS) was produced by acid leaching the olivine in 3M H_2SO_4 solution at 80 ± 5 °C for 1.5 h. The resultant suspension was then centrifuged at 4000 rpm for 1.5 min to extract APS [7].

The chemical compositions of CEM I (containing ~3 wt.% gypsum and ~5 wt.% limestone), APS, and LS, were determined by X-ray fluorescence (XRF) after lithium borate fusion and are given in Table 1. The relatively high loss on ignition of APS is attributed to the release of physically bound water and dehydroxylation of olivine impurities (e.g. clinochlore, chabazite, cordierite), as shown via TGA-MS and Q-XRD in our previous study [7]. The specific surface area (SSA Micromeritics 3Flex 3500), and density (AccuPyc II 1340 pycnometer) were determined and are also included in Table 1. The SSA was determined using N_2 adsorption–desorption with the Brunauer–Emmett–Teller method, while density was measured using helium gas displacement based on Boyle's law. The particle size distribution of CEM I, APS, and LS were determined by laser diffraction (Malvern Mastersizer 3000), and the particle size distribution of the sand was determined by sieve analysis, and this data is presented in Fig. 1.

2.2. Mix design and sample preparation

A total of 47 cement paste and mortar mixes were prepared for characterisation and performance testing. The mix designs of paste samples are given in Table 2 and mortar samples in Table 3. All mixes were prepared at a constant water-to-binder (w/b) ratio of 0.5. The reference paste and mortar without any additions are labelled "PC" and "PCM" respectively. The blended mixes contained a CEM I:APS mass ratio of 8:2. This was selected based on our previous study [7] that showed 20 wt.% APS as the maximum effective replacement level, ensuring sufficient availability of portlandite to sustain pozzolanic reaction and achieve comparable 28-day strength to the control Portland cement system. Further addition of APS causes significant workability loss (due to increased water demand), porosity increase and dilution effect which reduces strength. Limestone powder was incorporated at varying levels (0, 5, 10, 15, and 20 wt.% binder). These are denoted as "LS*x*" (for pastes) or "LSM*x*" (for mortars) where *x* refers to the limestone powder content in wt.% . Mixes with an additional 2 wt.% gypsum are labelled with suffix "A". Mortars had sand-to-binder mass ratio of 3:1. Superplasticiser dosages were varied between 0 and 2 wt.% binder.

Pastes were mixed using a mini-vortex mixer. To ensure homogeneity, the dry powders were initially mixed with the mini-vortex mixer for 3 min. Following water addition, the mixture was further homogenised by vortex mixing for 2 min and manual mixing for 1 min, before casting into 20 × 20 × 20 mm^3 cubes with vibration applied to remove entrapped air. The cubes were then covered with damp cloth and plastic membrane, demoulded after 24 h, and placed into a climate chamber at 20 ± 2 °C, 95 ± 5% RH. The paste samples were crushed to fine powder using an agate mortar and pestle after curing for 3 and 28 days, with further hydration inhibited by solvent exchange using isopropanol [25, 26]. The powdered samples were stored in near-vacuum condition (0.2 bar) with soda lime and silica gel to prevent carbonation, prior to TGA and XRD analysis.

Mortars were mixed using a planetary mixer (NG-AutoDigiMix 2). Dry ingredients were first blended at low speed and after 30 s, water was gradually added. Mixing continued for 90 s at low speed, followed by 30 s of manual mixing and 90 s of high-speed mixing. The fresh mortar was

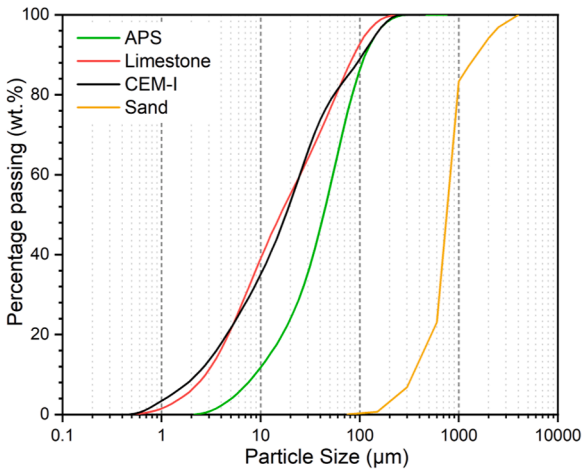


Fig. 1. Particle size distribution of CEM I, APS, limestone powder and sand.

Table 2
Mix design of cement paste samples.

Mix	CEM I (g)	APS (g)	LS (g)	Gypsum (g)	Water (g)	SP (%)	w/b
PC	100.0	0.0	0.0	0, 2	50	0	0.5
LS0	80.0	20.0	0.0	0	50	0, 2	0.5
LS5	76.0	19.0	5.0	0	50	0, 2	0.5
LS10	72.0	18.0	10.0	0	50	2	0.5
LS15	68.0	17.0	15.0	0	50	2	0.5
LS20	64.0	16.0	20.0	0	50	2	0.5
LS0A	78.4	19.6	0.0	2	50	0, 2	0.5
LS5A	74.5	18.6	4.9	2	50	0, 2	0.5
LS10A	70.6	17.6	9.8	2	50	2	0.5
LS15A	66.6	16.7	14.7	2	50	2	0.5
LS20A	62.7	15.7	19.6	2	50	2	0.5

Table 1
Chemical composition, specific surface area and density of CEM I, APS, and LS.

	Composition (%)										SSA	Density
	CaO	SiO_2	Al_2O_3	Fe_2O_3	SO_3	MgO	K_2O	Others	LOI	Total	(m^2/g)	(kg/m^3)
CEM-I	60.2	20.4	6.52	2.40	5.54	0.39	0.79	0.52	3.20	100.0	2.33	3040
APS	-	78.2	0.54	0.85	2.50	5.72	-	1.43	10.9	100.1	238	2216
LS	94.7	2.32	1.30	0.64	0.10	0.44	0.10	0.3	-	99.9	0.79	2790

Table 3
Mix design of mortar samples.

Mixes	Cement (g)	APS (g)	LS (g)	Gypsum (g)	Water (g)	Sand (g)	SP (%)	w/b
PCM	1000.0	0.0	0	0	500	3000	0	0.5
LSM0	800.0	200.0	0	0	500	3000	0, 1, 2	0.5
LSM5	760.0	190.0	50	0	500	3000	0, 1, 2	0.5
LSM10	720.0	180.0	100	0	500	3000	0, 1, 2	0.5
LSM15	680.0	170.0	150	0	500	3000	0, 1, 2	0.5
LSM20	640.0	160.0	200	0	500	3000	0, 1, 2	0.5
LSM0A	784.0	196.0	0	20	500	3000	0, 1, 2	0.5
LSM5A	744.8	186.2	49	20	500	3000	0, 1, 2	0.5
LSM10A	705.6	176.4	98	20	500	3000	0, 1, 2	0.5
LSM15A	666.4	166.6	147	20	500	3000	0, 1, 2	0.5
LSM20A	627.2	156.8	196	20	500	3000	0, 1, 2	0.5

tested for workability and cast into 50×50×50 mm^3 cubes in steel moulds and compacted on a vibration table until no air bubbles were released. Samples were covered with damp cloth and plastic membrane, demoulded after 24 h, and cured in a water bath at 20 ± 2 °C for up to 90 days prior to compressive strength testing.

2.3. Hydration kinetics

The effect of APS, LS and gypsum on the hydration kinetics of cement paste samples were investigated using isothermal conduction calorimeter (TA Instruments TAM Air). The mixes tested are given in Table 2 with PC used as a control reference. Mix LS0, LS5, LS0A and LS5A were also tested without superplasticiser to study changes in hydration kinetics. The mixing procedure followed that used for the preparation of cement paste cubes, as described in Section 2.2. Immediately after mixing, 10 g of the paste was transferred into the calorimeter and monitored at 20 °C for 7 days, following BS EN 196–11 [27]. Deionised water with equivalent heat capacity was used as a reference. All samples were tested three times, with heat flow and cumulative heat release recorded and normalized to the binder mass (CEM I + APS + LS + gypsum) in the mix.

Setting time was determined on pastes using an automatic Vicat apparatus (Controls Vicamatic3) following ASTM C191–21 [28]. 650 g of binder was mixed with 325 g of water according to the mix designs in Table 2. The freshly mixed paste was transferred into a cylindrical mould (70⌀mm × 40 mm) with the smoothed surface placed under the Vicat needle. The initial set was determined as the time taken for the needle to achieve a penetration of 25 mm, while the final set was determined when the needle did not penetrate the sample and resulted in only an incomplete circular impression on the surface.

2.4. Phase assemblage

Thermogravimetric analysis (TGA) was used to determine the portlandite and bound water content in paste samples using a simultaneous thermal analyser (Netzsch STA449 F5). 50 ± 0.1 mg of the powdered paste sample was placed in an Al_2O_3 crucible and heated to a maximum temperature of 1050 °C at a heating rate of 20 K/min with constant N_2 gas flowing 50 ml/min to maintain an inert environment. The bound water content was determined as the mass loss < 600 °C, while the portlandite content, $CH_{measured}$, was determined from the mass loss between 420 and 520 °C using tangential method [26,29]. To assess portlandite consumption associated with pozzolanic reactivity, the $CH_{theoretical}$ content was estimated by proportionally scaling the reference portlandite content according to the Portland cement fraction within the mixture [7]. This approach assumes that portlandite formation is directly proportional to cement content and does not explicitly account for potential changes in hydration kinetics arising from APS and limestone addition, such as nucleation and acceleration effects. Nevertheless, it provides a first-order approximation that enables comparative evaluation of portlandite consumption across the different blends.

Quantitative X-ray diffraction (Q-XRD, Malvern Panalytical Empyrean) was used to characterise crystalline phases. 0.9 g of powdered paste sample was mixed with 0.2 g corundum (Al_2O_3) as an internal standard, and this was ground with agate mortar and pestle for 20 min to ensure homogeneity. Quantitative phase analysis was performed using the Rietveld refinement method implemented in HighScore Plus software with the ICDD database. The internal standard (corundum) was used to enable quantification of both crystalline and amorphous phases. The sample was analysed using Cu Kα radiation at 45 kV and 40 mA. Diffraction data were recorded between 5° and 90° 2θ, with a step size of 0.02° per second. The degree of hydration was calculated as the ratio of the remaining mass of anhydrous cement phases in the hydrated paste, as identified by Q-XRD, to the initial cement content in the mix.

2.5. Workability and compressive strength

The workability of mortar mixes (Table 3) was assessed using a flow table (BS-EN 12,350–5:2019). Flow table measurements were repeated three times for each mix at 7 min ± 30 s after the binder was mixed with water. Mortar cubes (50×50×50 mm^3) were tested for uniaxial compressive strength at 1, 3, 7, 28 and 90 days using an automated compression machine (Controls Automax 5). The loading rate was maintained at 0.3 MPa/s. For each mix, three specimens were tested, and the average compressive strength is reported.

2.6. Scanning electron microscopy

The microstructure of pastes was examined using scanning electron microscopy (SEM). The 20 mm cube samples were cut into a 10 mm thick block using Buehler Isomet 1000 precision saw to reveal the 20×20 mm cross-section. The sections were immersed in isopropanol for up to 5 days and dried at 40 °C to constant mass [25] and then stored in a desiccator over silica gel and soda lime for up to 72 h to remove residual solvent. Subsequently, the dried sections were vacuum-impregnated with low-viscosity epoxy resin at 2.5 bars above atmospheric pressure, polished and carbon-coated (Emitech K550X sputter coater) [30]. SEM imaging used an 8.5 mm working distance and 15 kV acceleration voltage. Backscattered electron (BSE) images were acquired at a resolution of 1024 × 768 pixels with pixel spacing of 0.182 μm/pixel at 500x magnification. Secondary electron (SE) images were also obtained at 3000× magnification and a resolution of 1024 × 768 pixels to observe the change in morphology of ettringite within the cement matrix.

Porosity was determined by image analysis using the overflow pore segmentation method [31]. The brightness histogram was extracted from each BSE image using ImageJ and converted into cumulative histogram (grey value against segmented area). The upper greyscale threshold value for pores was determined from the inflection point on the cumulative histogram using the intersection of two tangential lines. A correction factor of 0.8 was applied to the threshold to match segmented pore areas [31]. Porosity was determined as the average pore area fraction calculated from 30 BSE images for each sample.

3. Results

3.1. Hydration kinetics

Heat flow and cumulative heat release data for cement pastes containing APS, limestone, and gypsum are shown in Fig. 2. PC was used as the control to evaluate the effects of APS, and limestone and gypsum addition. All data are normalised to total binder mass.

The control PC paste exhibited a peak heat flow of 3.40 mW/g at ~8.2 hours (Fig. 2a) and cumulative heat release of 282 J/g after 72 hours (Fig. 2b). Incorporating 20 wt.% APS and 2 wt.% superplasticiser (LS0) reduced and delayed the main hydration peak and decreased the cumulative heat. This is due to clinker dilution by APS and retardation caused by the superplasticiser. However, comparing LS0 to a similar mix without superplasticiser (LS0N) shows that the retardation effect of superplasticiser is short term and does not affect the cumulative heat at later ages.

Increasing limestone content from 5 to 20 wt.% (LS5–LS20) further reduced hydration peak intensity and cumulative heat due to clinker dilution. The position of the main peak remained unchanged, indicating that limestone does not delay hydration. LS5 had a slightly earlier and higher peak heat flow than LS0. The cumulative heat data show that LS5 achieved similar values to LS0, despite having reduced clinker content. This may be attributed to the synergistic effect of limestone and APS. However, this trend was not observed in samples containing additional gypsum.

Fig. 2(c) and (d) present the corresponding heat of hydration data for pastes containing an additional 2 wt.% gypsum. As expected, PCA (control paste with 2 wt.% gypsum) showed a broader and lower intensity main peak than PC. The presence of additional gypsum delays early reaction of tricalcium aluminate (C_3A) by promoting ettringite formation and suppressing hydration. As a result, the cumulative heat released by 72 hours was slightly lower than the PC control.

Similar effects can be seen in the APS-limestone blends with additional gypsum (LS0A–LS20A). The main hydration peak became broader with higher limestone content, with a distinct shoulder corresponding to C_3A hydration. This shows that gypsum moderates aluminate reactions, producing clear separation between the C_3S and C_3A peaks [19–22]. As with the non-gypsum series, cumulative heat decreased at higher limestone additions, though the reduction was less pronounced, suggesting that gypsum partially compensated for the effect of clinker dilution.

Mixes without superplasticiser (LS0N, LS5N, LS0AN, LS5AN) showed markedly different hydration behaviour. These exhibited significantly higher and earlier heat flow peaks compared to samples containing superplasticiser. This is consistent with previous research where nanosilica or silica enhanced early-age hydration kinetics [6,24,32,33]. Despite the increased initial heat evolution, cumulative heat values were similar for samples with and without superplasticiser by 72 h (Fig. 2b and d).

Fig. 3 shows the initial and final setting times of pastes. The PC mix had initial setting at 295 min and final setting at 371 min. LS0 recorded similar values to PC. This shows that incorporating 20 wt.% APS and 2

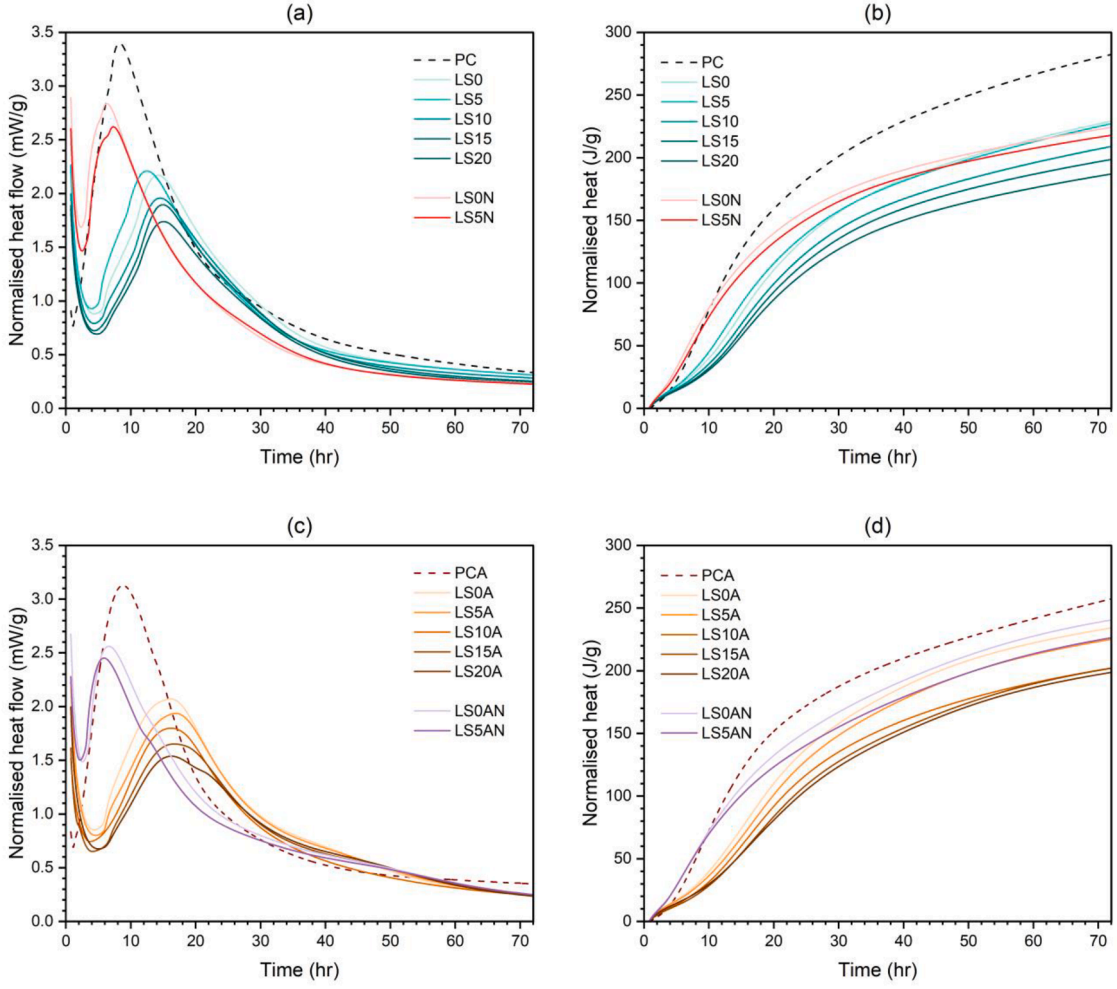


Fig. 2. (a) Heat flow and (b) cumulative heat release for pastes with 20 wt.% APS and 0–20 wt.% limestone; (c) heat flow and (d) cumulative heat release for pastes with 2 wt.% gypsum addition. Data is normalised to total binder mass. Mixes labelled 'N' contain no superplasticiser.

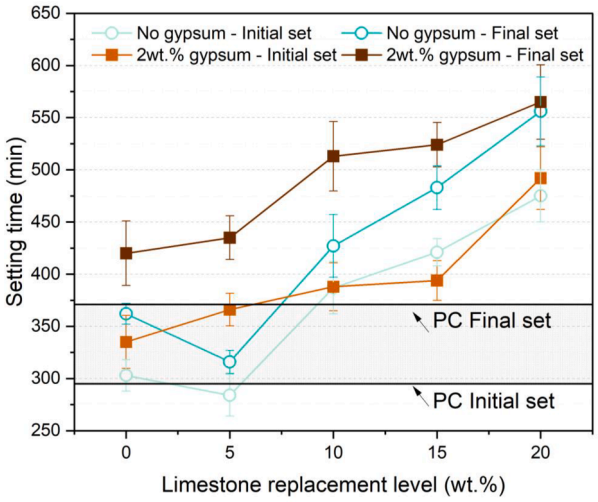


Fig. 3. Initial and final setting times of pastes. The error bars represent standard error of setting time.

wt.% superplasticiser did not significantly influence setting time. LS5 showed slightly more rapid setting and a shorter setting interval as observed in the calorimetry data. As limestone content increased, both initial and final setting times increased. Mixes with an additional 2 wt.% gypsum followed the same trend, with progressively longer setting times at higher limestone contents. The results are broadly consistent with the isothermal conduction calorimetry data, in which the induction period ends after approximately six hours of hydration, marking the transition to the acceleration stage. This period also corresponds to the onset of initial paste setting.

3.2. Phase assemblage

Fig. 4a) and b) show the results from TGA of pastes at 3-days and 28-days of hydration. Three major mass loss events can be seen, corresponding to the dehydration of C-S-H, AFt and AFm phases (40–200 °C), dehydroxylation of portlandite (420–520 °C) and decomposition of calcium carbonate (600–850 °C) [26,34]. The calculated contents of bound water, portlandite and calcium carbonate (from TGA) and degree of hydration (from Q-XRD) are given in Table 4 and 5, respectively.

As expected for PC samples, longer curing led to greater total mass loss, reflecting a higher degree of hydration. In the low-temperature region (40–200 °C), the DTG deepens from 3 days to 28 days across all series, consistent with increased bound water loss from C–S–H and AFt/AFm dehydration. The portlandite content remained stable, while calcium carbonate shows a slight reduction. This is probably due to the reaction between limestone and residual C_3A phase forming mono- or hemicarbonate.

Mixes containing APS show an increase in mass loss between 40 and 200 °C, together with a reduced CH peak at 420–520 °C compared with PC. This was also confirmed from Table 4, where $CH_{measured}$ is significantly lower than $CH_{theoretical}$ across all samples containing APS. This indicates additional C–S–H formation by pozzolanic reaction of APS with portlandite, which increases bound water and reduces CH. Table 4 shows that the pozzolanic reaction of APS occurred early (< 3 days), and the difference between portlandite content of mixes containing APS and

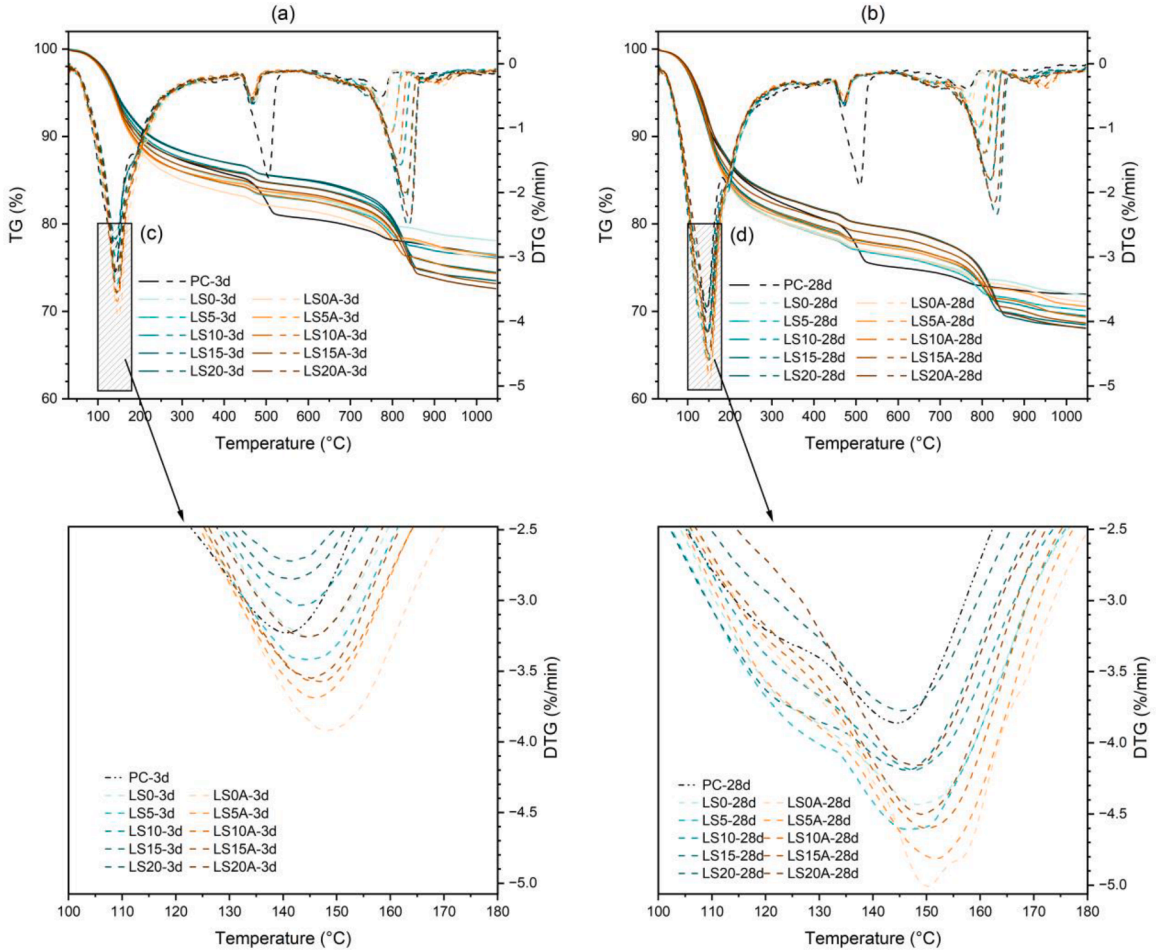


Fig. 4. (a, b) TGA of 3-day and 28-day hydrated cement pastes, with enlarged DTG (boxed) showing dehydration of C-S-H gel and Aft.

Table 4
CH theoretical, CH measured and bound water of 3-day and 28-day hydrated cement pastes containing APS, limestone and gypsum.

Mixes	3 Days			28 Days		
	$CH_{Theoretical}$ (wt.%)	$CH_{Measured}$ (wt.%)	Bound water (wt.%)	$CH_{Theoretical}$ (wt.%)	$CH_{Measured}$ (wt.%)	Bound water (wt.%)
PC	15.5 ± 1.27	15.5 ± 1.27	19.4	15.4 ± 3.18	15.4 ± 3.18	25.0
LS0	12.4 ± 0.08	4.02±0.09	17.0	12.3 ± 0.09	3.47±0.12	23.6
LS5	11.8 ± 0.04	3.82±0.06	17.4	11.7 ± 0.13	4.07±0.17	23.8
LS10	11.2 ± 0.07	4.25±0.10	15.8	11.1 ± 0.12	3.85±0.17	22.9
LS15	10.5 ± 0.06	4.60±0.09	15.1	10.5 ± 0.08	4.30±0.12	22.6
LS20	9.91±0.03	4.94±0.05	15.0	9.89±0.09	4.45±0.14	20.6
LS0A	12.1 ± 0.04	3.45±0.06	18.5	12.1 ± 0.04	2.72±0.05	23.6
LS5A	11.5 ± 0.06	3.34±0.08	16.8	11.5 ± 0.08	2.89±0.10	22.9
LS10A	10.9 ± 0.03	3.52±0.04	17.3	10.9 ± 0.06	3.13±0.09	22.5
LS15A	10.3 ± 0.02	3.90±0.04	16.6	10.3 ± 0.05	3.25±0.07	21.6
LS20A	9.72±0.05	4.36±0.08	15.9	9.66±0.08	4.13±0.13	20.6

Table 5
Breakdown of AFm content shown in Fig. 6.

Mixes	AFm content (%)			
	3 days		28 days	
	Hemicarbonate	Monocarbonate	Hemicarbonate	Monocarbonate
PC	0.2	0	0.6	1.8
LS0	0.1	0.0	0.5	0
LS5	0.0	0.0	0.9	0
LS10	0.2	0.0	0.6	0.1
LS15	0.1	0.0	0.9	0.3
LS20	0.3	0.0	0.6	0.4
LS0A	0.0	0.0	0.1	0.0
LS5A	0.0	0.0	0.0	0.0
LS10A	0.0	0.0	0.2	0.0
LS15A	0.0	0.0	0.3	0.0
LS20A	0.0	0.0	0.4	0.0

PC increase at 28 days, showing that pozzolanic reactions continues beyond early ages.

Increasing limestone content increases the mass loss in the carbonate region (600–850 °C). The bound water (40–200 °C) and CH content tend to decrease with increasing limestone content because of clinker dilution, which reduces the absolute volume of clinker-derived hydrates. $CH_{measured}$ increases as the limestone replacement increases. This may be because of the hydration enhancement triggered by the presence of limestone [14,15,35]. A small reduction in the intensity of the carbonate decarbonation peak at 28-days relative to 3 day is also observed for several mixes. This reflects partial conversion of calcite into carboaluminate phases through reaction with dissolved aluminates. This reduces the weight loss in the 600–850 °C range and shifts some mass loss to lower temperatures, where AFm dehydration occurs. The effect is modest, which suggests that only a limited fraction of the limestone participates in these reactions.

With additional gypsum, the TG and DTG curves of 3-day samples show slightly higher mass loss at ~100–200 °C, consistent with greater AFt formation and retention (see Fig. 4). At later ages, bound water contents were also broadly similar between the two series (~ 20–24 wt. %), indicating comparable total hydrate formation. The CH peak of samples with extra gypsum is consistently lower than that of corresponding mixes without gypsum. This is coherent with the values $CH_{measured}$ displayed in Table 4. At 28 days, $CH_{measured}$ ranged from 2.7 wt.% (LS0A) to 4.1 wt.% (LS20A), compared with 3.5–4.4 wt.% in the mixes without gypsum (LS0–LS20). The slightly lower CH in the gypsum-containing blends, together with higher Aft-related mass loss, suggests that additional gypsum promoted the persistence of sulphate-rich phases while marginally reducing portlandite availability.

The X-ray diffraction patterns at 28 days (Fig. 5) show that the phase assemblage consists of hydration products, residual clinker phases, carbonates and olivine residues. The identified hydration products include calcium hydroxide, ettringite and AFm–CO_3 phases (hemicarbonate and monocarbonate) present in limestone-containing systems. Calcite is observed as the main carbonate phase associated with limestone filler. In addition, some residual clinker phases, mainly alite (C_3S) and belite (C_2S), are detected. No crystalline phases attributable to APS are identified, consistent with its amorphous nature.

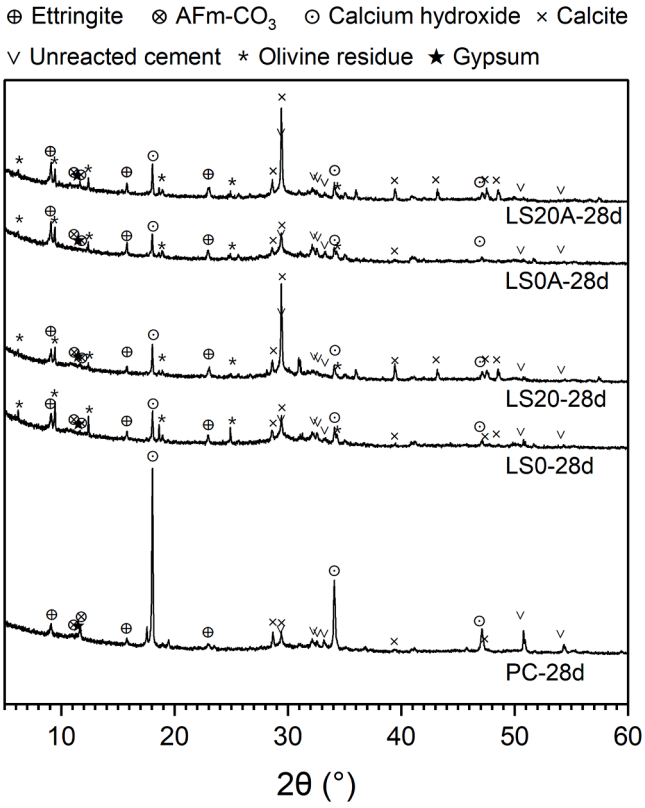


Fig. 5. XRD pattern of 28-days PC, LS0, LS20, LS0A and LS20A.

Fig. 6 shows the Q-XRD data for hydrated cement pastes at 3-day and 28-day. The trends are consistent with the TGA data. For all mixes, the amorphous phase fraction increased with curing age, while unreacted cement phases (C_3S, C_2S, C_3A, C_4AF) decreased with continued hydration. APS-containing mixes showed reduced portlandite content compared to PC because of pozzolanic reaction. A small amount of olivine residues (e.g. clinochlore, enstatite, chabazite and cordierite) remained within the hydrated paste, indicating low reactivity of these phases in the APS. The fluctuation in olivine residue reflects the phase inconsistency of raw materials and APS [7]. Mixes with added limestone powder showed increased calcite content while unreacted cement

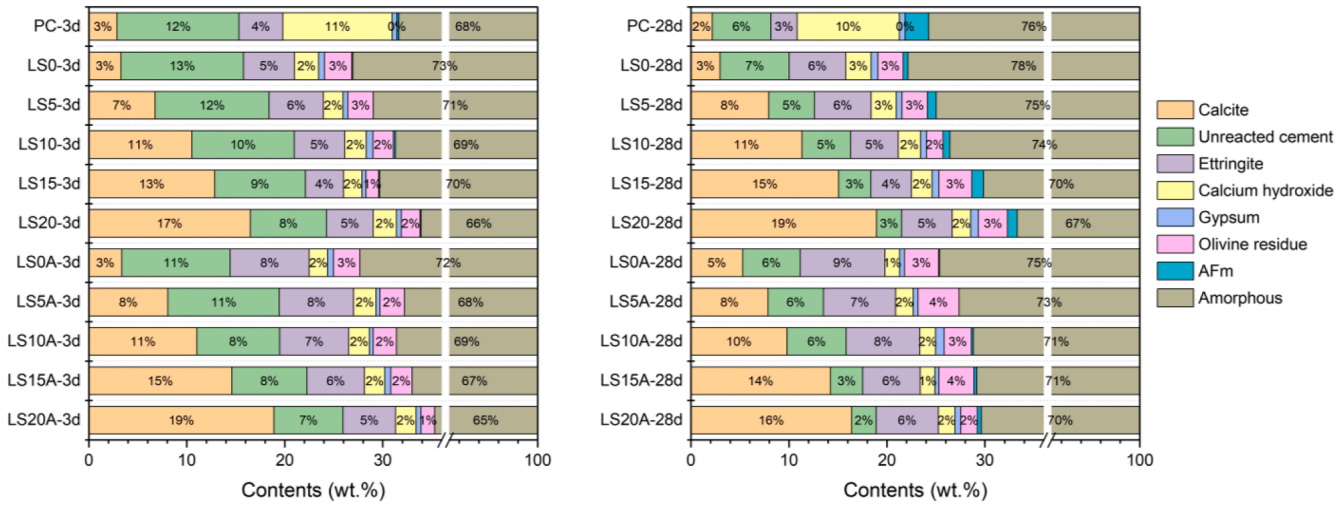


Fig. 6. Q-XRD phase assemblage of a) 3-day and b) 28-day hydrated cement pastes.

phases decreased due to dilution, consistent with the mix proportions (Table 2). Small quantities of hemi- and monocarbonate AFm phases were detected in samples containing limestone and APS, with monocarbonate predominantly observed in the 28-day samples (Table 5).

Mixes containing additional gypsum showed increased ettringite content, confirming that gypsum promotes ettringite formation by regulating aluminate reactivity. At 28-days, the ettringite content remained relatively stable, with minor quantities of hemicarbonate AFm phase detected in gypsum-containing samples, indicating that most ettringite was retained. Samples with additional gypsum had reduced portlandite content.

Table 6 shows that the degree of hydration increased from 3 to 28 days for all mixes, indicating continued hydration with time. The degree of hydration also increased with increasing limestone content. This suggests that the presence of fine limestone enhanced hydration by providing additional nucleation sites that promote early hydrate formation. Mixes with additional gypsum (LS0A–LS20A) followed the same trend, with values closely matching those without gypsum at both ages. The similarity between the two series indicates that gypsum addition did not significantly alter the overall hydration degree for the range of limestone contents investigated.

3.3. Workability

Fig. 7 shows flow table data for all mortar mixes with varying superplasticiser dosages. The control mix (PCM) exhibited a spread of 116 mm. The inclusion of APS significantly reduced workability due to high specific surface area and increased water demand. The use of superplasticiser alone was insufficient to mitigate this problem. LSM0, with 2 wt.% superplasticiser, achieved only a 104 mm spread. However, substituting cement with 5 – 20 wt.% of limestone significantly improved the flow particularly when combined with superplasticiser addition. For example, LSM15 and LSM20 with 2 wt.% superplasticiser achieved comparable flow to PCM, suggesting that the presence of limestone powder helps redistribute water in the mortar and improves workability. Similar phenomena were observed for mortar samples containing additional gypsum, with LSM15A and LSM20A having comparable flow properties to PCM.

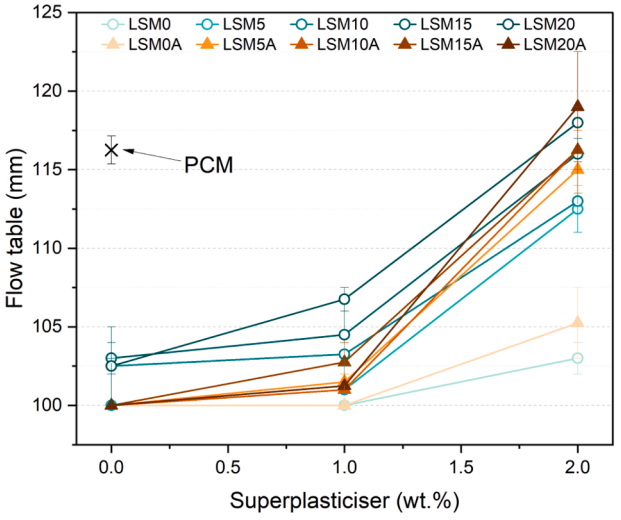


Fig. 7. Effect of superplasticiser addition on flow table values of mortars. Error bars represent standard error.

Table 6
Degree of hydration of cement pastes after curing for 3 and 28 days.

Mixes	Degree of hydration (%)	
	3-day	28-day
PC	84.2	93.5
LS0	83.5	90.7
LS5	83.8	93.1
LS10	84.7	92.1
LS15	85.3	94.6
LS20	87.7	95.4
LS0A	85.5	92.3
LS5A	84.4	92.2
LS10A	87.7	91.2
LS15A	88.2	94.1
LS20A	88.5	95.5

3.4. Compressive strength

Fig. 8 shows the compressive strength data for mortar samples. The strength of the control mortar (PCM) increases with age due to continued hydration. The strength of PCM increases rapidly before 28 days, reaching ~50.6 MPa. Strength development after 28 days was relatively low with samples achieving 56.3 MPa at 90 days.

Samples with 20 wt.% APS replacement level (LSM0) has a slower early strength development, achieving ~29.2 MPa at 3 days. At 7 days and beyond, LSM0 had higher compressive strengths than PCM, with ~60.0 MPa at 90 days. This suggests that at early ages, the dilution caused by the APS impeded initial strength development. However, at

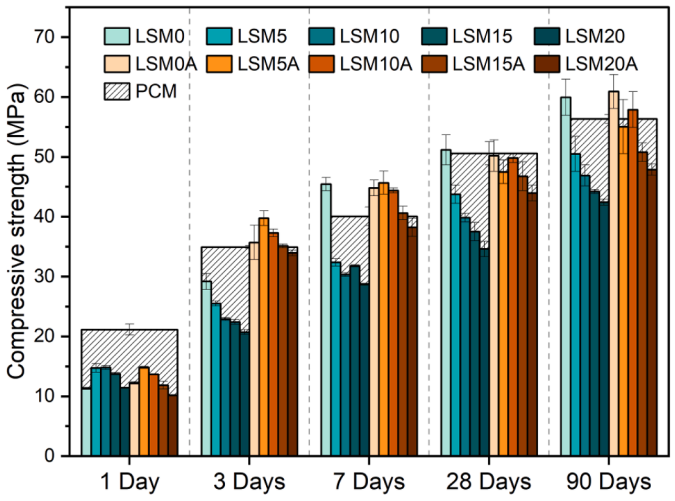


Fig. 8. Compressive strength of mortar samples containing amorphous precipitated silica with varying limestone and gypsum content at 1, 3, 7, and 28-days. Error bars represent standard error.

later ages, the pozzolanic reaction of APS helps refine the microstructure, resulting in higher compressive strengths than the control mortar.

When limestone is incorporated (LSM5–LSM20), the compressive strength remains lower than PCM at all ages, with a clear decrease as the limestone content increases. At 1-day, the limestone-bearing samples show slightly higher strength than LSM0, suggesting that limestone provides some early hydration acceleration. This early effect does not extend to later ages, as the combination of limestone and cement does not improve strength development. The results indicate that limestone alters the balance of reactions in the APS–PC system by replacing clinker and reducing the phases available for strength formation.

Adding gypsum (LSM0A–LSM20A) shifts the strength profile of the system. At 1-day, strengths are similar to mixes without gypsum but lower than PCM. From 3-days onwards, a clear improvement occurs, with LSM5A and LSM10A reaching around 39.7 and 37.3 MPa at 3 days, matching or exceeding PCM and the non-gypsum samples. After 7-days, mixes containing 5–10% limestone with gypsum reach ~44.4–45.7 MPa, comparable to LSM0 and higher than PCM. By 28 and 90 days, LSM0A, LSM5A and LSM10A converge around the PCM values of ~55.0–60.9 MPa. The higher limestone blends (LSM10A–LSM20A) show limited reduction in strength compared to LSM5–LSM20. These results indicate that ettringite formation promoted by additional gypsum refines the microstructure in the APS–limestone–PC system. This helps mixes recover the later-age strength that is reduced when only limestone is used.

3.5. Microstructure

Fig. 9 shows SEM images of selected samples (LS5A, LS20 and LS20A). Fig. 7(a) is the microstructure of LS5A at 3 days, showing a range of identifiable phases, including unhydrated cement clinker, limestone, APS, portlandite, and C–S–H gel. Clinochlore was also detected as a major impurity associated with APS. Other impurities were not observed, because of low concentrations. At this age, numerous unhydrated clinker particles and dark porous regions are evident. No distinct hydration rims were seen around clinker particles. This indicates that while dissolution of clinker occurred, nucleation and growth of C–S–H may occur on the high-surface-area APS particles and limestone rather than on clinker surfaces [36,37]. This is consistent with seeding effect, in which pozzolanic additives promote decentralised C–S–H formation, shifting nucleation sites away from cement grains.

The SEM–SE images (Fig. 8b and c) show regions from 28-day LS20 and LS20A pastes. Both show dense clusters of acicular ettringite crystals occupying pore space and linking adjacent hydrates. Gypsum is no longer visible as discrete particles because it has reacted with aluminate phases to form ettringite. In LS20A ettringite needles are more densely intergrown to form rosette-like clusters, indicating extensive sulphate reaction and pore-filling.

Fig. 10 shows image analysis data of porosity. At 3 days, PC exhibits one of the lowest pore area fractions at ~11.3%. The introduction of APS increases porosity due to reduced workability and reactions, while increasing limestone content further increases the pore area fraction. In contrast, samples with 2 wt.% gypsum exhibit consistently lower pore fractions. At this age, LS20 shows the highest value (15.8%), followed by LS20A (12.4%). At 28-days, all samples show a reduction in pore area fraction as hydration and pozzolanic reactions continue. LS0A and LS5A achieve the lowest values (5.9% and 6.6% respectively), highlighting the combined benefits of APS and gypsum in refining porosity.

4. Discussion

The behaviour of the CEM I–APS blends reflects a balance between accelerated hydration, fresh-state properties, microstructure development, and pozzolanic reaction. The high specific surface area of APS provides additional nucleation sites and adsorption capacity that may affect sulphate balance. This is evidenced by the reduced dormant period, the earlier main peak in the heat of hydration data (Fig. 2), and accelerated aluminate reactions. TGA and Q-XRD show reduced portlandite and increased bound water in APS-containing mixes, confirming sustained pozzolanic reaction and continued C–S–H formation beyond 3 days. However, the high surface area that accelerates hydration also increases water demand, reduces workability and is associated with a higher pore fraction at early ages. The replacement of clinker with APS gives comparable long-term microstructure and strength but detrimental to fresh state properties and early porosity. These must be managed through careful mix design.

Limestone modifies this balance mainly through chemical and physical effects. At low replacement levels, limestone acts as a fine filler that provides additional nucleation surfaces for hydrate growth, improving early hydration behaviour. This is consistent with the higher degree of hydration observed with increasing limestone content. Limestone also improves the flow properties at a constant w/b, indicating a redistribution of mixing water within the paste and mortar. This effect is particularly important for APS-containing mixes, where the high surface area of APS reduces workability. At high limestone replacement levels clinker dilution dominates. The reduction in clinker content lowers the total amount of hydrates forming and increases porosity, leading to a systematic decrease in strength with increasing limestone content. Although 3- and 28-days samples shows formation of hemi- and monocarboante, the pore-filling phases were insufficient to compensate for the strength loss. The data shows that limestone supports early hydration and workability but cannot recover later-age strength when clinker replacement exceeds ~10 wt.% in APS-containing systems.

These results also show that limestone behaves differently in the presence of APS compared with conventional Portland cement systems. In ordinary systems, low limestone levels often support later-age strength through improved particle packing and the formation of carbonate–aluminate phases [15,35,38]. In the APS-containing system, limestone appears to primarily act as a physical filler, causing a dilution effect. However, some degree of interaction with APS cannot be excluded, which may contribute to the early-age performance. This may explain why the benefits of limestone addition are mainly observed at early ages, while strength decreases with increasing replacement levels.

Gypsum introduces an additional level of control by regulating sulphate availability and the timing of C_3A hydration. Its presence broadens and slightly reduces the intensity of the main hydration peak, while also producing a clearer separation between C_3S- and C_3A-related features. TGA and Q-XRD results show higher contents of ettringite in gypsum-containing mixes at both 3 and 28 days. The retention of ettringite is

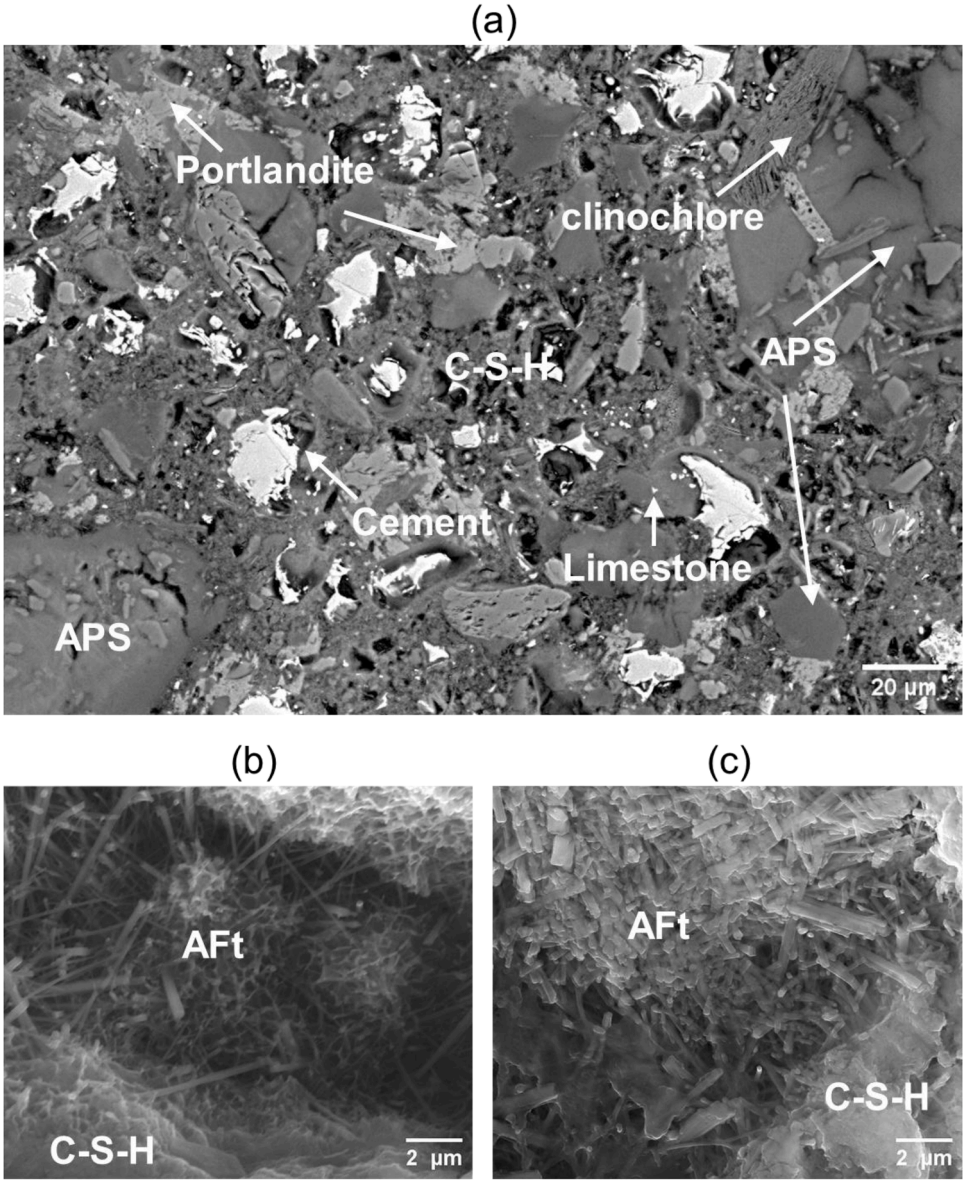


Fig. 9. (a) SEM–BSE image of 3-day LS5A paste showing unhydrated cement, limestone, APS, portlandite, C–S–H gel, and clinochlore (APS impurity). SEM–SE images of ettringite in 28-day (b) LS20 and (c) LS20A pastes, respectively.

governed by aluminate availability, carbonate presence, and sulphate concentration. In Portland cement systems, C_3A initially reacts with sulphate to form ettringite, which remains stable as long as sufficient sulphate is available. Upon sulphate depletion, ettringite becomes unstable and can convert to AFm phases, such as monosulphate or, in the presence of carbonate, hemi- or monocarbonate. The addition of gypsum increases sulphate concentration in the pore solution, thereby stabilising ettringite and inhibiting its conversion to AFm phases, which explains the reduced AFm formation in these mixes. SEM observations further confirm dense networks of acicular ettringite infilling pore space. Image analysis indicates lower pore fractions in these systems, particularly in blends containing APS and low to moderate limestone contents. This suggests that gypsum sustains ettringite as a stable pore-filling phase over the time scale of this study, contributing to pore refinement and improved strength. However, the influence of gypsum becomes less pronounced at higher limestone replacement levels, where reduced clinker content limits overall hydrate formation and the extent to which additional ettringite can enhance the microstructure.

The mechanical response is consistent with these hydration and microstructural observations. APS-only blends reach or exceed the strength of the Portland cement reference at later ages because of lower portlandite content and increasing amorphous phase. Limestone additions reduce strength at all ages when used without gypsum, reflecting the combined effects of clinker dilution and slightly higher porosity. When gypsum is added, early strength recovers, and later strength matches or closely approaches the reference mortar for blends with low to moderate limestone content. Mixes with 5–10 wt.% limestone and gypsum show the strongest agreement between hydration behaviour, microstructure and mechanical properties. These samples exhibit refined pore structures, sustained ettringite and degrees of hydration comparable to or higher than the limestone-free APS blend, with strengths the same as the control at 28 and 90 days. This multiscale consistency lends support to the proposed mechanisms.

This research shows that quaternary blends of Portland cement, APS, limestone, and gypsum can be designed to achieve workability and strength comparable to the reference cement while reducing clinker content. With 2 wt.% gypsum, a limestone replacement of 10 wt.% gives the most balanced behaviour, improving hydration through filler and

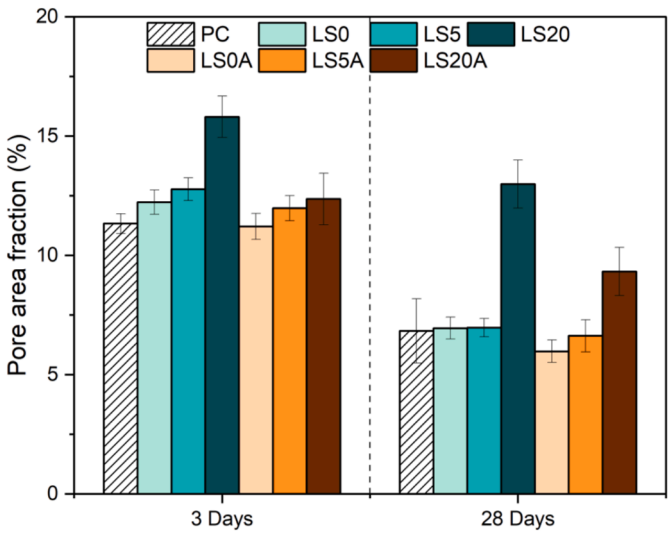


Fig. 10. Pore area fraction of cement pastes at 3 and 28 days, determined via BSE image analysis. Error bars represent standard error.

seeding effects without compromising long-term strength. From a sustainability perspective, the combined use of APS and limestone reduces clinker use and lowers embodied carbon while maintaining appropriate fresh and hardened properties. This approach offers a practical route to achieve low-carbon cement, and it is consistent with global sustainability goals to reduce carbon emissions associated with construction and infrastructure development.

However, several limitations of the present study should be acknowledged. In TGA for example, the use of sample mass at 600 °C to indicate complete dehydration is an approximation, as minor amount of bound water may be released at higher temperatures. Consequently, $CH_{measured}$ content may be overestimated and should be considered when interpreting the results. The degree of hydration derived from Q-XRD should be interpreted with caution. Hydration involves the incorporation of water into reaction products, altering mass relative to the original anhydrous binder and introducing an uncertainty in the calculated values. Nevertheless, the results provide a reasonable approximation for comparative purposes, and the observed trends between mixes are considered reliable. Furthermore, the pore segmentation in BSE image analysis was conducted on two-dimensional cross-sectional images, which has limited resolution and does not fully represent the three-dimensional pore structure. Complementary techniques, such as gas adsorption, mercury intrusion porosimetry or X-ray computed tomography, would be required for a more complete characterisation of porosity and pore connectivity.

From a durability perspective, the observed phase assemblage has several important implications for long-term performance. The addition of gypsum suppressed the early formation of both monosulphate and hemi-/monocarbonate phases. The limited formation of AFm phases, particularly monosulphate, may influence chloride binding capacity. Therefore, it is important to consider the long-term stability of ettringite and its potential transformation into AFm phases. Furthermore, the reduced portlandite content and increased C–S–H formation associated with APS incorporation may enhance resistance to calcium leaching and improve microstructural stability. However, the lower portlandite content also reduces buffering capacity against carbonation. Consequently, while the phase assemblage observed here is beneficial for early and medium-term performance, further assessment of carbonation resistance, sulphate stability, and chloride transport/binding is required to fully evaluate the durability of this binder system.

From a practical perspective, the feasibility of APS-based binders at scale must be considered. Their broader application will depend on the availability of suitable raw materials, as well as the ability to produce and supply APS in sufficient quantities within existing cement manufacturing and distribution systems. Further techno-economic and life cycle assessments are therefore required to evaluate the viability of this approach for large-scale implementation.

5. Conclusions

Amorphous precipitated silica (APS) derived from olivine can be incorporated with limestone and gypsum to form a quaternary binder capable of reducing clinker content while maintaining satisfactory fresh and hardened state properties. The performance of these blends is determined by the balance between clinker availability and the physical effects introduced by APS and limestone, with gypsum controlling early aluminate reactions and pozzolanic reaction supporting the formation of stable pore-filling hydrates. A blend containing CEM I:APS at 8:2 mass ratio, 10 wt.% limestone and 2 wt.% gypsum shows the most consistent performance, achieving workability and strengths comparable to the Portland cement reference. The research shows that APS-based quaternary binders offer a practical route for clinker reduction without compromising key engineering properties. Further assessment of long-term durability is required to confirm the suitability of these low-carbon cements for broader application.

CRediT authorship contribution statement

Pei B. Ong: Writing – original draft, Visualization, Methodology, Investigation, Formal analysis, Data curation. **Chenyang Li:** Investigation, Formal analysis. **Christopher Cheeseman:** Writing – review & editing, Visualization, Supervision. **Hong S. Wong:** Writing – review & editing, Visualization, Supervision, Resources, Project administration, Funding acquisition, Conceptualization.

Declaration of competing interest

The authors declare that they have no known competing financial interests or personal relationships that could have appeared to influence the work reported in this paper.

Acknowledgements

The research leading to this publication benefitted from funding by the Department for Energy Security and Net Zero (DESNZ), under project number CCUS 2106 of the CCUS Innovation 2.0 call – part of the Net Zero Innovation Portfolio (NZIP), EPSRC funding under grant number EP/R010161/1 and from support from the UKCRIC Coordination Node, EPSRC grant number EP/R017727/1, which funds UKCRIC's ongoing coordination. Open access fee for this article was paid from the Imperial College London Open Access Fund. The authors would like to thank Yixiu Zhuge, Noel Djobo and Jianhang Feng for their technical support and general discussions.

Data availability

Data will be made available on request.

References

[1] B. Shanks, C. Howe, S. Draper, H. Wong, C. Cheeseman, Carbon capture and storage in low-carbon concrete using products derived from olivine, R. Soc. Open. Sci. 11 (2024), https://doi.org/10.1098/RSOS.231645.
[2] B. Shanks, C. Howe, S. Draper, H. Wong, C. Cheeseman, Production of low-carbon amorphous SiO2 for use as a supplementary cementitious material and nesquehonite from olivine, Mater. Lett. 361 (2024) 136133, https://doi.org/10.1016/J.MATLET.2024.136133.
[3] A. Scott, C. Oze, V. Shah, N. Yang, B. Shanks, C. Cheeseman, A. Marshall, M. Watson, Transformation of abundant magnesium silicate minerals for enhanced CO 2 sequestration, Commun. Earth .Environ. 2 (2021), https://doi.org/10.1038/s43247-021-00099-6.

[4] A. Lazaro, H.J.H. Brouwers, G. Quercia, J.W. Geus, The properties of amorphous nano-silica synthesized by the dissolution of olivine, Chem. Eng. J. 211-212 (2012) 112–121, https://doi.org/10.1016/J.CEJ.2012.09.042.
[5] Y.X. Chen, S. Li, B. Mezari, E.J.M. Hensen, R. Yu, K. Schollbach, H.J.H. Brouwers, Q. Yu, Effect of highly dispersed colloidal olivine nano-silica on early age properties of ultra-high performance concrete, Cem. Concr. Compos. 131 (2022) 104564, https://doi.org/10.1016/j.cemconcomp.2022.104564.
[6] V. Shah, A. Scott, Pozzolanic characteristics of silica recovered from olivine, Constr. Build. Mater. 332 (2022) 127378, https://doi.org/10.1016/J.CONBUILDMAT.2022.127378.
[7] P.B. Ong, Y. Zhuge, C. Cheeseman, H.S. Wong, Production and properties of amorphous silica extracted from olivine for use as a supplementary cementitious material, Cement 23 (2026) 100168, https://doi.org/10.1016/j.cement.2025.100168.
[8] N. Raza, W. Raza, S. Madeddu, H. Agbe, R.V. Kumar, K.H. Kim, Synthesis and characterization of amorphous precipitated silica from alkaline dissolution of olivine, RSC. Adv. 8 (2018) 32651–32658, https://doi.org/10.1039/c8ra06257a.
[9] T. Ding, H. Wong, M. Yio, C. Cheeseman, Production of amorphous aluminosilicate and vaterite from acid leaching of hydrated cement paste, J. Sustain. Cem. Based. Mater. 13 (2024) 1502–1513, https://doi.org/10.1080/21650373.2024.2397484.
[10] E.A. Gorrepati, P. Wongthahan, S. Raha, H.S. Fogler, Silica precipitation in acidic solutions: mechanism, pH effect, and salt effect, Langmuir 26 (2010) 10467–10474, https://doi.org/10.1021/la904685x.
[11] D. Wang, C. Shi, N. Farzadnia, Z. Shi, H. Jia, A review on effects of limestone powder on the properties of concrete, Constr. Build. Mater. 192 (2018) 153–166, https://doi.org/10.1016/J.CONBUILDMAT.2018.10.119.
[12] M. Zajac, A. Rossberg, G. Le Saout, B. Lothenbach, Influence of limestone and anhydrite on the hydration of Portland cements, Cem. Concr. Compos. 46 (2014) 99–108, https://doi.org/10.1016/J.CEMCONCOMP.2013.11.007.
[13] F. Zunino, K. Scrivener, The reaction between metakaolin and limestone and its effect in porosity refinement and mechanical properties, Cem. Concr. Res. 140 (2021) 106307, https://doi.org/10.1016/J.CEMCONRES.2020.106307.
[14] W. Huang, H. Kazemi-Kamyab, W. Sun, K. Scrivener, Effect of cement substitution by limestone on the hydration and microstructural development of ultra-high performance concrete (UHPC), Cem. Concr. Compos. 77 (2017) 86–101, https://doi.org/10.1016/J.CEMCONCOMP.2016.12.009.
[15] M. Zajac, A. Rossberg, G. Le Saout, B. Lothenbach, Influence of limestone and anhydrite on the hydration of Portland cements, Cem. Concr. Compos. 46 (2014) 99–108, https://doi.org/10.1016/J.CEMCONCOMP.2013.11.007.
[16] M. Sharma, S. Bishnoi, F. Martirena, K. Scrivener, Limestone calcined clay cement and concrete: a state-of-the-art review, Cem. Concr. Res. 149 (2021) 106564, https://doi.org/10.1016/J.CEMCONRES.2021.106564.
[17] B. Kanagaraj, N. Anand, U.J. Alengaram, R. Samuvel Raj, S. Karthick, Limestone calcined clay cement (LC3): a sustainable solution for mitigating environmental impact in the construction sector, Resour. Conserv. Recycl. Adv. 21 (2024) 200197, https://doi.org/10.1016/J.RCRADV.2023.200197.
[18] J. Sun, F. Zunino, K. Scrivener, Hydration and phase assemblage of limestone calcined clay cements (LC3) with clinker content below 50 %, Cem. Concr. Res. 177 (2024) 107417 https://doi.org/10.1016/J.CEMCONRES.2023.107417.
[19] T. Huang, Q. Yuan, F. He, Y. Xie, Understanding the mechanisms behind the time-dependent viscoelasticity of fresh C3A–gypsum paste, Cem. Concr. Res. 133 (2020) 106084, https://doi.org/10.1016/J.CEMCONRES.2020.106084.
[20] A. Quennoz, K.L. Scrivener, Hydration of C3A–gypsum systems, Cem. Concr. Res. 42 (2012) 1032–1041, https://doi.org/10.1016/J.CEMCONRES.2012.04.005.
[21] T. Huang, Q. Yuan, S. Zuo, Y. Xie, C. Shi, New insights into the effect of gypsum on hydration and elasticity development of C3S paste during setting, Cem. Concr. Res. 159 (2022) 106860, https://doi.org/10.1016/J.CEMCONRES.2022.106860.
[22] G. Geng, R.J. Myers, Y.S. Yu, D.A. Shapiro, R. Winarski, P.E. Levitz, D.A. L. Kilcoyne, P.J.M. Monteiro, Synchrotron X-ray nanotomographic and spectromicroscopic study of the tricalcium aluminate hydration in the presence of gypsum, Cem. Concr. Res. 111 (2018) 130–137, https://doi.org/10.1016/J.CEMCONRES.2018.06.002.
[23] X. Dai, M. Yio, H. Wu, S.B. Lopez, C. Cheeseman, H.S. Wong, Enhancing the rheology, reaction kinetics and early-age strength of limestone calcined clay cement (LC3) with sodium silicate addition, Cem. Concr. Res. 198 (2025) 107997, https://doi.org/10.1016/J.CEMCONRES.2025.107997.
[24] J.N.Y. Djobo, S. Draper, B. Shanks, H. Wong, C. Cheeseman, Reactivity of olivine-derived amorphous silica and its potential for use as a supplementary cementitious material, J. Build. Eng. 114 (2025) 114379, https://doi.org/10.1016/J.JOBE.2025.114379.
[25] R.O.S.J. Chwast, zlem Cizer Nele De Belie Yuvaraj Dhandapani Pawel Durdzinski Jan Elsen Johannes Haufe Doug Hooton Cédric Patapy Manu Santhanam Karen Scrivener Didier Snoeck Laurent Steger Sui Tongbo Anya Vollpracht Frank Winnefeld, Barbara Lothenbach, N. Alderete, C. Andrade, S.A. Bernal, L. Buffo-Lacarrière, J. Chwast, zlem Cizer, L. Courard, N. De Belie, C. Dedeloudis, E. Denarié, Y. Dhandapani, J. Duchesne, P. Durdzinski, J. Elsen, M. Geiker, E. Gruyaert, J. Haufe, D. Herfort, D. Hooton, M.G. Juenger, H. Justnes, S. Kamali-Bernard, A.J. Klemm, K. Kovler, M. Kozhukhova, B. Lothenbach, J.F. Martirena-Hernandez, T. Matschei, E.M. Méndez, T. Nawa, V.T. Nguyen, A. Nunes, C. Patapy, J.L. Provis, J. Sanjayan, M. Santhanam, K. Scrivener, K.K. Sideris, R. Snellings, D. Snoeck, M. Soutsos, L. Steger, T. Sui, Y.V. Zaccardi, J. Visser, A. Vollpracht, F. Wang, F. Winnefeld, G. Ye, M. Zervaki, J. Zhou, S.R.Z. Snellings, J.J.C.Á. Elsen, N.D.D.B.Á. Snoeck, Y.M.D.Á. Santhanam, P.K.D.Á. Scrivener, RILEM TC-238 SCM recommendation on hydration stoppage by solvent exchange for the study of hydrate assemblages, Mater. Struct. 51 (2018), https://doi.org/10.1617/s11527-018-1298-5.
[26] Y. Zhuge, P.B. Ong, H.S. Wong, R.J. Myers, Natural fibre-enhanced CO2 transport and uptake in cement pastes subjected to enforced carbonation, J. CO2 Util. 90 (2024) 102983, https://doi.org/10.1016/J.JCOU.2024.102983.
[27] British Standards Institution, BS EN 196-11:2018 Methods of Testing Cement - Heat of hydration. Isothermal Conduction Calorimetry method, 2019, London, doi:10.3403/30361319U.
[28] ASTM International. ASTM C191-21: Standard Test Methods for Time of Setting of Hydraulic Cement By Vicat Needle, West Conshohocken, PA, 2021, https://doi.org/10.1520/C0191-21.
[29] K. Scrivener, R. Snellings, B. Lothenbach. A Practical Guide to Microstructural Analysis of Cementitious Materials, 1st ed., CRC Press, Taylor & Francis Group, 2018 https://doi.org/10.1201/b19074.
[30] H.S. Wong, N.R. Buenfeld, Patch microstructure in cement-based materials: fact or artefact? Cem. Concr. Res. 36 (2006) 990–997, https://doi.org/10.1016/J.CEMCONRES.2006.02.008.
[31] H.S. Wong, M.K. Head, N.R. Buenfeld, Pore segmentation of cement-based materials from backscattered electron images, Cem. Concr. Res. 36 (2006) 1083–1090, https://doi.org/10.1016/J.CEMCONRES.2005.10.006.
[32] P. Feng, H. Chang, X. Liu, S. Ye, X. Shu, Q. Ran, The significance of dispersion of nano-SiO2 on early age hydration of cement pastes, Mater. Des. 186 (2020) 108320, https://doi.org/10.1016/J.MATDES.2019.108320.
[33] X. Liu, L. Liu, K. Lyu, T. Li, P. Zhao, R. Liu, J. Zuo, F. Fu, S.P. Shah, Enhanced early hydration and mechanical properties of cement-based materials with recycled concrete powder modified by nano-silica, J. Build. Eng. 50 (2022) 104175, https://doi.org/10.1016/J.JOBE.2022.104175.
[34] H. Sun, J. Qian, Y. Yang, C. Fan, Y. Yue, Optimization of gypsum and slag contents in blended cement containing slag, Cem. Concr. Compos. 112 (2020) 103674, https://doi.org/10.1016/J.CEMCONCOMP.2020.103674.
[35] K. Vance, M. Aguayo, T. Oey, G. Sant, N. Neithalath, Hydration and strength development in ternary portland cement blends containing limestone and fly ash or metakaolin, Cem. Concr. Compos. 39 (2013) 93–103, https://doi.org/10.1016/J.CEMCONCOMP.2013.03.028.
[36] X. Li, J. Bizzozero, C. Hesse, Impact of C-S-H seeding on hydration and strength of slag blended cement, Cem. Concr. Res. 161 (2022) 106935, https://doi.org/10.1016/J.CEMCONRES.2022.106935.
[37] R. Hari, Y. Zhuge, M. KM, Performance assessment of pervious concrete incorporated with calcium silicate hydrates (C-S-H) cultivated on rice husk ash substrates – A trend surface analysis interpretation, Constr. Build. Mater. 446 (2024) 138050, https://doi.org/10.1016/J.CONBUILDMAT.2024.138050.
[38] J. Bizzozero, K.L. Scrivener, Limestone reaction in calcium aluminate cement–calcium sulfate systems, Cem. Concr. Res. 76 (2015) 159–169, https://doi.org/10.1016/J.CEMCONRES.2015.05.019.